IDBP: Image Dehazing Using Blended Priors Including Non-local, Local, and Global Priors

Mingye Ju, Can Ding, *Member, IEEE,* Wenqi Ren, *Member, IEEE,* and Yi Yang

***Abstract*—In this letter, a robust and promising atmospheric scattering model (ASM)-based image dehazing technique called IDBP is developed, which overcomes the intrinsic limitation of available techniques based on single priors. It consists of two modules, i.e., an atmospheric light estimation (ALE) module and a multiple prior constraint (MPC) module. The ALE module is based on a new global brightening strategy of enhancing the brightness of image with minimum information loss. The MPC smartly blends the constrains of non-local prior, local prior, and global prior to shrink the solution space of haze removal, which avoids the limitation of using any single priors. Unlike previous works, IDBP does not require any training process, but is based on multiple priors and minimal information loss principle to impose the ASM, thereby making it easy to implement and ensuring its robustness. Numerous experiments reveal that the proposed IDBP outperforms the state-of-the-art alternates.**

***Index Terms*—Atmospheric Scattering Model, Atmospheric Light Estimation, Multiple Priors Constrains, Image Dehazing**

I. Introduction

IMAGES taken in hazy weather are usually interfered by turbid impurities suspended in atmosphere, which leads to low contrast and dim color. Because of the poor visual quality, the deteriorated images cannot be used in vision applications that need high-quality inputs [1]. The degraded images due to haze need to be dehazed and efficient restoration technologies are desired.

In early days, haze removal was realized by directly employing traditional enhancement methods to improve the local or global contrast of a hazy image. Despite its simplicity, the recovery quality is limited as the image degradation theory is not considered. To make up for this deficiency, a fusion strategy of blending multiple traditional image enhancement methods [2], [3] was proposed. Compared to preliminary work, recently published dehazing algorithms have achieved great success, and they can be roughly grouped into two categories: prior-based techniques and data-driven techniques.

This work was supported by National Natural Science Foundation of China (61902198) and Natural Science Foundation of Jiangsu Province (BK20190730). (*Corresponding authors: Can Ding)*

M. Ju is with the School of Internet of Things, Nanjing University of Posts and Telecommunications, Nanjing, 210000, China. e-mail:(Jumingye@njupt.edu.cn)

C. Ding is with the Global Big Data Technologies Centre (GBDTC), University of Technology Sydney (UTS), Ultimo, NSW, 2007, Australia. e-mail:(Can.Ding@uts.edu.au)

W. Ren is with the State Key Laboratory of Information Security, Institute of Information Engineering, Chinese Academy of Sciences, Beijing, 100000, China. e-mail:(renwenqi@iie.ac.cn)

Y. Yang is with the Centre for Artificial Intelligence (CAI), University of Technology Sydney (UTS), Ultimo, NSW, 2007, Australia. e-mail:(Yi.Yang@uts.edu.au)

Prior-based Techniques: Its core idea is to impose a handcraft prior on atmospheric scattering model (ASM) to extract imaging parameters, and then the haze-free result can be restored using these parameters. Mathematically, the ASM can be modeled by

$$\boldsymbol{I}(x,y) = \boldsymbol{A} \cdot \boldsymbol{\rho} \cdot t(x,y) + \boldsymbol{A} \cdot (1 - t(x,y)), \tag{1}$$

where $\boldsymbol{I}$ is the hazy image, $\boldsymbol{A}$ is the atmospheric light, $\boldsymbol{\rho}$ is the scene albedo or haze-free image, and t is the transmission related to scene depth. Depending on the manner of finding transmission, this type of method can be further divided into pixel-wise [4], [5], patch-wise [6], [7], non-local-wise [8], and global-wise [9] strategies. In general, these strategies all have some advantages for specific examples. However, they are not able to deal with all practical situations since they are based on single prior and each prior inevitably has some limitations.

Data-driven Techniques: The data-driven techniques are to establish dehazing systems by learning or extracting effective haze-related features from synthetic datasets. These techniques can be classified into convolutional neural networks (CNN) wise [10]–[15] and generative adversarial network (GAN) wise [16]–[18] strategies according to the networks they used. Despite the fact that these systems are capable of removing the haze for most cases, they also have some drawbacks, e.g., unable to deal with dense haze and needs numerous training samples. Moveover, data-driven makes the dehazing process like a "black box", thus less domain knowledge can be involved in the learning procedure to further improve the performance.

Moreover, for current ASM-based dehazing methods, either prior-based or data-driven ones, their atmospheric light was estimated according to haze-related features or networks trained by synthetic dataset [19]. However, some special types of real-world images do not meet the premises to do so and thus leading to color cast or dim effect in the restored results.

In this letter, a novel ASM-based image dehazing method named IDBP is developed. The proper fusion of multiple priors including local, non-local, and global priors rather than only one prior can effectively avoid the shortness of any single prior. Moreover, the proposed IDBP utilizes a new method to calculate the atmospheric light, which is able to maximize the average brightness while avoiding excessive information loss. The combination of this new atmospheric light estimation method and multiple-prior-based strategy makes IDBP an excellent dehazing method that exhibits higher robustness than available methods.

II. Proposed Methodology

This section describes the proposed simple yet effective dehazing technique, IDBP. It only consists of two modules, i.e., an atmospheric light estimation (ALE) module and a multiple prior constraint (MPC) module for scene restoration.

A. Atmospheric Light Estimation (ALE) Module

ALE is one of key steps to achieve high-quality haze removal. The effectiveness of ALE is closely related with the quality of restored images. Atmospheric light can be located from sky or heavy haze regions [6], [20] by using haze-related features. However, this approach is invalid when such regions are not visible in the image. Another strategy advocated in [8], [21] is to utilize haze-line prior or patch-repeatability prior to calculate atmospheric light. Although this strategy is not limited by the presence of sky or heavy haze regions, the estimation errors are unavoidable once the input hazy images cannot fully meet the premise of the adopted priors.

By moving $\boldsymbol{A}$ to the left side of the equation, Eq. (1) can be rewritten as

$$\boldsymbol{I}'(x,y) = \frac{\boldsymbol{I}(x,y)}{\boldsymbol{A}} = \boldsymbol{\rho} \cdot t(x,y) + 1 - t(x,y). \tag{2}$$

In practice, $\boldsymbol{A} = [A^R, A^G, A^B]$ is introduced to correct the atmospheric light of the input hazy image to be [1,1,1], aiming to ensure that the corrected image $\boldsymbol{I}'$ has sufficient light to expose the textures and contours. In addition, it also helps to avoid color cast in the recovered result, which will be illustrated later in Section III-B. It can be concluded from Eq. (2) that a smaller $\boldsymbol{A}$ leads to a brighter $\boldsymbol{I}'$, but too small $\boldsymbol{A}$ would result in pixels overflow, thus information loss (IL). To find the optimal value of $\boldsymbol{A}$, a global brightening (GB) strategy is designed. The key idea is to make the hazy image as bright as possible while sacrificing minimum IL. Formally, the ALE based on GB strategy is defined as

$$A_p^c = \underset{A^c}{argmin}\{\Psi(max(min(\frac{I^c}{A^c}, 1), 0)) - \tau\}, \tag{3}$$

where A_p^c is the searched optimal atmospheric light, $c \in \{R, G, B\}$ is the color channel index, $\tau = 0.015$ is the pre-set IL ratio, and $\Psi(\cdot)$ stands for IL ratio operator, i.e., calculating the percentage of pixels that are completely black or white. Note that Eq. (3) is a simple 1-D convex optimization task and can be easily solved by golden section method. Different from previous works, the designed ALE is not rely on any prior knowledge or training process, but is based on the whole image to calculate the atmospheric light by following the principle of minimum information loss. The benefit of doing so is that ALE can have the highest level to expose the textures and contours, while preventing information loss and underexposure.

B. Multiple Prior Constraint (MPC) Module

As well-known, imposing only one image prior on ASM to realize haze removal may lead to haze residue, over-enhancement, and over-saturation phenomenon in recovery results. This is because single prior inevitably has some limitations for certain types of hazy images. To remedy the limitation of any single prior, a MPC module that merges the ideas of three priors is proposed. With the proper fusion procedure, the three priors are jointly imposed on ASM during dehazing process, thus the solution space of haze removal can be accurately shrunk, leading to fascinating haze-free results.

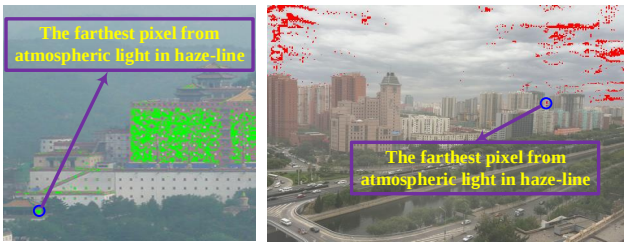

Fig. 1. Two examples to illustrate the drawback of haze-line prior. In these pictures, pixels with same color indicate the haze-line.

1) Describe transmission using non-local prior: Relying on a key observation that an image usually contains many similar colors (non-local prior), Berman et. al [8] recognize each set of distinct colors termed as haze-line via spherical coordinates and then calculate the transmission by assuming that the farthest pixel in each haze-line from the atmospheric light is haze free. This leads to the following equation

$$t(x,y) = \frac{r(x,y)}{r_{i-max}}, \quad (x,y) \in \Omega_i, \tag{4}$$

where $i \in [1, 2, ..., n]$ is the index of haze-line, Ω_i is the coordinate set of the i^{th} haze-line, $r = \|\boldsymbol{I} - \boldsymbol{A}_p\|$, and $r_{i-max} = \{max(r(x,y)), (x,y) \in \Omega_i\}$. Note that this assumption is not always reliable to all haze-lines in a given image. For example, as shown in Fig. 1, the farthest pixels from the atmospheric light in the highlighted haze-lines are obviously not haze-free. Therefore, in this work, a coefficient κ_i is introduced to Eq. (4) to make a more accurate estimation of the transmission, which yields

$$t(x,y) = \kappa_i \cdot \frac{r(x,y)}{r_{i-max}}, \quad (x,y) \in \Omega_i. \tag{5}$$

It should be pointed out that although Eq. (5) exhibits a higher accuracy and is more robust, the extra parameter κ_i increases the complexity of haze removal.

2) Reducing solution set of transmission using local prior: According to local prior [6], an input image can be divided into several non-overlapping patches (in this work, the patch size is selected to be 15×15) and the transmissions in a local patch can be regarded as a constant. Considering the fact that an image can be divided into n haze-lines according to non-local prior or m patches according to the local prior, there could be an overlap between the i^{th} haze-line and the j^{th} patch. In this case (when $\Phi_j \cap \Omega_i \neq \emptyset$), according to Eq. (5), the transmission of the j^{th} patch can be calculated as

$$t'(j) = \kappa_i \cdot \frac{r(x,y)}{r_{i-max}}, \quad (x,y) \in \Phi_j \cap \Omega_i \neq \emptyset \tag{6}$$

where $t'(j)$ and Φ_j represent the transmission value and coordinate index of the j^{th} patch. Performing a mean operation on Eq. (6) within the area of $\Phi_j \cap \Omega_i$ leads to

$$t'(j) = \kappa_i \cdot M_{j,i} \tag{7}$$

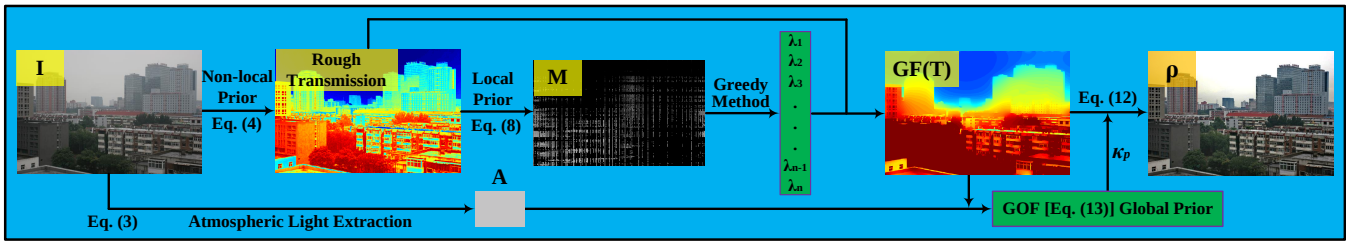

Fig. 2. The flow chart of the proposed IDBP.

and

$$M_{j,i} = \frac{1}{|\Phi_j \cap \Omega_i|} \cdot \sum_{(x,y)\in\Phi_j\cap\Omega_i} \frac{r(x,y)}{r_{i-max}}, \tag{8}$$

where $|\Phi_j \cap \Omega_i|$ is the number of non-empty coordinates in the intersection $\Phi_j \cap \Omega_i$. Taking the case that the i^{th} haze-line and the j^{th} patch are not overlapped also into consideration, a complete $m \times n$ matrix representing the average transmission of the pixels in the overlapped area $\Phi_j \cap \Omega_i$ is obtained as

$$N(j,i) = \begin{cases} t'(j) = \kappa_i \cdot M_{j,i}, & \Phi_j \cap \Omega_i \neq \emptyset \\ \emptyset, & \Phi_j \cap \Omega_i = \emptyset \end{cases}. \tag{9}$$

Note that M can be calculated by traversing all patches and all haze-lines according to Eq. (8). Meanwhile, according to local prior, the average transmissions of the j^{th} patch should be a constant, i.e., $N(j,1) = N(j,2) = N(j,i) = ... = N(j,n)$ as long as there is an overlap between the j^{th} patch and the designated haze-line. These attributes enable us to employ a greedy approach [22] to seek a suitable ratio of κ_i and κ_1, where

$$\kappa_i = \lambda_i \cdot \kappa_1, \qquad i \in [1, 2, ..., n]. \tag{10}$$

Combining Eq. (5) and Eq. (10), the transmission map can be expressed by

$$t = \kappa_1 \cdot \mathrm{GF}(T) = \kappa_1 \cdot \mathrm{GF}\left(\lambda_i \cdot \frac{r(x,y)}{r_{i-max}}\right), \quad (x,y) \in \Omega_i, \tag{11}$$

where guided filter $\mathrm{GF}(\cdot)$ is introduced to blur the excessive texture [23].

3) Scene recovery using global prior: Substituting the atmospheric light $\boldsymbol{A}_p$ and Eq. (11) into Eq. (1), dehazing formula (DF) is obtained as

$$\boldsymbol{\rho}(x,y) = \mathrm{DF}(\kappa_i) = 1 + \frac{\boldsymbol{I}(x,y) - \boldsymbol{A}_p}{\boldsymbol{A_p} \cdot \kappa_1 \cdot \mathrm{GF}\,(T)}, \tag{12}$$

where T, $\boldsymbol{I}$, and $\boldsymbol{A_p}$ are all known, only κ_1 remains unsolved. To find out the best value for κ_1, a maximum information entropy (global prior)-based global optimization function (GOF) is provided as

$$\kappa_p = \underset{\kappa_1}{argmin}\{-\Theta(\mathrm{DF}\,(\kappa_1))\}, \tag{13}$$

where κ_p is the calculated optimal of κ_1 and $\Theta(\cdot)$ is an information entropy operator. Similar to Eq. (3), this GOF can be solved via golden section method. Once κ_p is attained, the haze-free result can be directly generated via Eq. (12).

For clarity, the flow chart of the proposed IDBP is illustrated in Fig. 2. The first step is to extract the atmospheric light using the proposed GB-based ALE. Then the input image is processed by non-local prior to attain a rough transmission, which is later further constrained by local prior to obtain an improved transmission map. Finally, combining the transmission blurred by guided filter and the estimated atmospheric light, haze-free result can be easily obtained via global prior-based optimization function.

III. Experiments

In this section, the atmospheric light estimated by IDBP was firstly compared with those obtained by other comparable techniques. Then, qualitative and quantitative comparisons were conducted between IDBP and other state-of-the-art algorithms, including DEFADE (TIP 2015) [3], NLD (TPAMI 2020) [8], GDN (ICCV 2019) [11], MSCNN (ECCV 2016) [10], MSBDN (CVPR 2020) [24], and EPDN (CVPR 2019) [16]. Note that the codes of these benchmark methods are available on the authors' GitHub. All experiments were conducted on the same PC with Intel(R) Core (Tm) i7-8700 CPU@ 3.20 GHz 16.00 GB RAM to ensure fairness.

A. Accuracy of Atmospheric Light Estimation

Unlike the exiting atmospheric light estimation methods, IDBP utilizes a global brightening module to calculate the atmospheric light, leading to a more promising performance. To illustrate this superiority, the estimation results obtained from the proposed IDBP and four classic approaches (DCP [6], NLD [8], ARAL [25], and IPR [21]) were compared on four challenging images, as shown in Fig. 3. Note that the ground truth of atmospheric light (GTAT) was manually marked to ensure accuracy. By comparing the extracted atmospheric light using different methods with the GTAT, it is observed that DCP, ARAL, and IPR fail for the first three examples, while NLD cannot work well on the third one. Moreover, all these comparable benchmark approaches lose utility when the sky or heavy haze is not visible (see the last example). On the contrary, the proposed IDBP avoids these interferences and attains a reliable atmospheric light for all the given examples.

B. Qualitative Comparison

1) Comparison on challenging real-world images: To illustrate the excellent performance of IDBP, we compared it against six state-of-the-art algorithms on three challenging real-world images with different haze levels. The selected hazy images and the results dehazed by different methods are shown in Fig. 4.

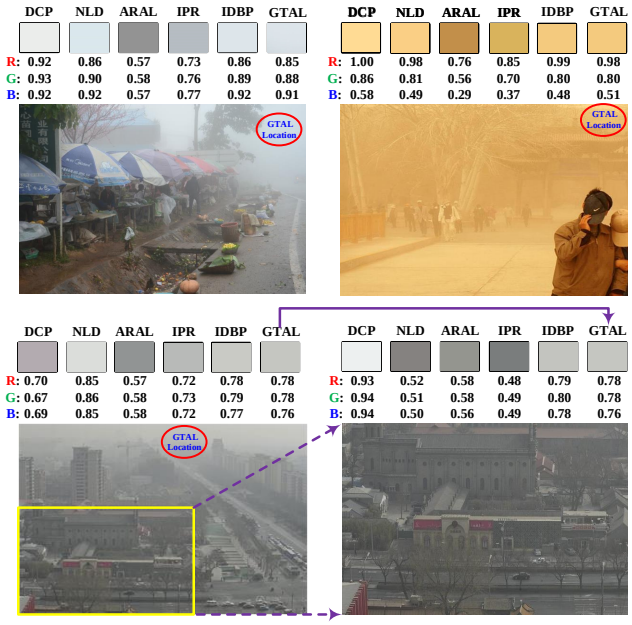

Fig. 3. Comparison of the extracted atmospheric light using DCP, NLD, ARAL, IPR, and IDBP, along with the manually extracted ground truth atmospheric light (GTAL).

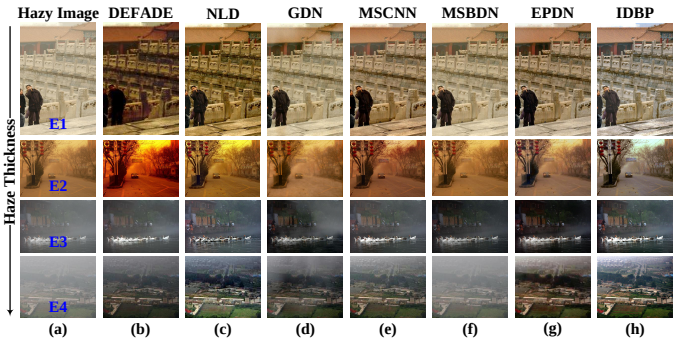

Fig. 4. Qualitative comparison of the state-of-the-art techniques on real-world images.

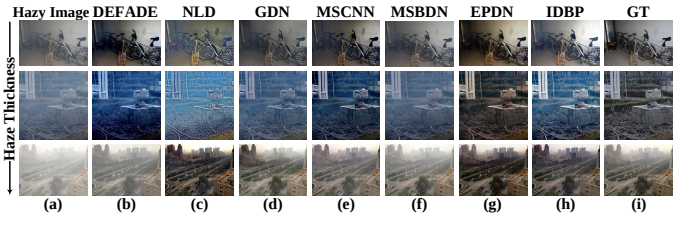

Fig. 5. Qualitative comparison of the state-of-the-art techniques on synthesis images.

As exhibited in Fig. 4(b), DEFADE performs well when dealing with the scenes covered in dense haze, whereas the results after haze removal appear to be too dark. For NLD shown in Fig. 4(c), it can restore necessary details and contours for the given examples, but is not able to handle gray scenes (see the first example). In Figs. 4(d) to 4(f), GDN, MSCNN, and MSBDN avoid this drawback and work well for misty images, but a small amount of haze is still visible in their dehazed results (see the third and last examples). It can be observed from Fig. 4(g) that EPDN is capable of thoroughly removing the haze for all the examples. However, the recovered results look darker than they should be, e.g., the tree in the last example. In addition, all the benchmark algorithms are ineffective for color cast images (see the second example). In contrast, the proposed IDBP circumvents all the limitations of these compared techniques, and can restore a promising haze-free result for different types of hazy images.

2) Comparison techniques on synthesized images: In subsequence, three dehazing datasets, i.e., SOTS [26], O-Haze [27], and I-Haze [28], consisting of both hazy images and their corresponding ground truth (GT), were tested to facilitate the comparison between IDBP and the state-of-the-art alternates. Note that each example the datasets were down-sampled to 1/4 of its original resolution in order to avoid running out of memory and to accelerate the evaluation. The results processed by different techniques on three representative images collected in these datasets are illustrated in Fig. 5.

According to Figs. 5(b) and 5(c), DEFADE and NLD are able to peel off the haze from hazy inputs, but their restored color seems to be over-saturated. As shown in Figs. 5(d) to 5(f), GDN, MSCNN, and MSBDN can produce fascinating results for the given misty images while they can not deal with the ones with heavy haze. As seen from Fig. 5(g), the haze cover is removed by EPDN but the results obviously look darker than the GT images. As a comparison, the proposed IDBP can well handle different complex situations and better reveal the potential textures shrouded in haze than other techniques.

C. Quantitative Comparison

The performance of IDBP is also assessed quantitatively and compared with other state-of-the-art techniques. Table I summarizes the scores of fog aware density evaluator (FADE) [3] and natural image quality evaluator (NIQE) [29] on the restoration results of the four real-world images shown in Fig. 4. Note that a smaller NIQE and FADE represent that the restored image is more realistic and has less mist residue, respectively. It can be concluded from Table I that IDBP either achieves the best or the second-best NIQE and FADE scores for all the examples. Furthermore, two commonly used indicators, i.e., peak signal to noise ratio (PSNR) and structural similarity (SSIM) [30], were used to quantitatively rank the recovery performance between IDBP and the six benchmark approaches on the three aforementioned datasets. In general, larger PSNR and SSIM stand for a stronger dehazing ability and a better structure maintenance, respectively. The PSNR and SSIM scores of different technologies on the three datasets are listed in Table II. It is clear that IDBP performs the best on I-Haze and O-Haze datasets and achieves the third-best score on SOTS. It worth to mention that the released codes of GDN and MSBDN were pre-trained with some images from RESIDE dataset (SOTS is a subset of RESIDE). This is why the performance of GDN and MSBND on SOTS is particularly high. Nevertheless, the actual haze-free results attained by IDBP are visually better than those obtained by GDN and MSBND, especially for the last example in Fig. 4.

TABLE I
QUANTITATIVE COMPARISON OF DIFFERENT TECHNIQUES ON THE IMAGES SHOWN IN FIG. 4 USING FADE AND NIQE (BEST: BOLD HIGHLIGHT, SECOND BEST: RED HIGHLIGHT).

Metric	Image	DEFADE	NLD	GDN	MSCNN	MSBDN	EPDN	IDBP
FADE	E1	**0.1435**	0.1556	0.3161	0.1833	0.4599	0.2050	0.1513
	E2	**0.1939**	0.2335	0.2926	0.2834	0.3191	0.3733	0.2259
	E3	1.4034	0.4667	0.5115	**0.3500**	0.8693	0.4054	0.3849
	E4	0.7931	0.3071	0.6020	0.4768	1.9304	0.3365	**0.2824**
NIQE	E1	4.3991	4.4767	4.0784	4.0297	4.0210	4.3058	**3.6756**
	E2	2.9497	2.7281	2.8944	2.8317	2.9033	3.1489	**2.5844**
	E3	4.0343	3.9518	3.4277	3.6347	3.6054	4.0473	**3.3229**
	E4	4.4232	4.5484	4.0359	4.4475	4.1739	3.7394	**3.5096**

TABLE II
QUANTITATIVE COMPARISON OF DIFFERENT TECHNIQUES ON I-HAZE, O-HAZE, AND SOTS DATASETS USING PSNR AND SSIM (BEST: BOLD HIGHLIGHT, SECOND BEST: RED HIGHLIGHT).

Dataset	Metric	DEFADE	NLD	GDN	MSCNN	MSBDN	EPDN	IDBP
I-HAZE	PSNR	15.9535	14.5387	16.0571	16.5441	16.699	15.4013	**17.1194**
	SSIM	0.7500	0.7197	0.6295	0.7783	0.7658	0.7192	**0.8053**
O-HAZE	PSNR	15.3412	13.3776	17.1057	16.6224	16.4633	16.8574	**17.4490**
	SSIM	0.6039	0.6094	0.3770	0.6917	0.6596	0.6793	**0.7418**
SOTS	PSNR	16.9045	18.5907	28.2819	16.9549	**33.666**	22.9536	23.4423
	SSIM	0.7498	0.8080	0.9704	0.7592	**0.9876**	0.7785	0.8705

IV. CONCLUSION

In this letter, a novel single image haze removal technique called IDBP is presented. Different from existing related algorithms, IDBP considers the atmospheric light estimation (ALE) as an equivalence of maximizing the average brightness of hazy image with sacrificing minimal information loss, which significantly improves the accuracy. Moreover, the multiple prior constraint (MPC) module used in IDBP effectively reduces the solution set of ASM, thereby resulting in a more promising restoration than the comparable methods. Both qualitative and quantitative experiments show that the proposed IDBP has a stronger capability to enhance visual quality of hazy image, retain richer details, and maintain color fidelity than state-of-the-art approaches.

REFERENCES

[1] Y. Y. Schechner and Y. Averbuch, "Regularized image recovery in scattering media," *IEEE Transactions on Pattern Analysis and Machine Intelligence*, vol. 29, no. 9, pp. 1655–1660, 2007.

[2] C. O. Ancuti, C. Ancuti, and P. Bekaert, "Effective single image dehazing by fusion," in *2010 IEEE International Conference on Image Processing*, 2010, pp. 3541–3544.

[3] L. K. Choi, J. You, and A. C. Bovik, "Referenceless prediction of perceptual fog density and perceptual image defogging," *IEEE Transactions on Image Processing*, vol. 24, no. 11, pp. 3888–3901, 2015.

[4] J. Wang, K. Lu, J. Xue, N. He, and L. Shao, "Single image dehazing based on the physical model and msrcr algorithm," *IEEE Transactions on Circuits and Systems for Video Technology*, vol. 28, no. 9, pp. 2190–2199, 2018.

[5] M. Ju, C. Ding, D. Zhang, and Y. J. Guo, "Bdpk: Bayesian dehazing using prior knowledge," *IEEE Transactions on Circuits and Systems for Video Technology*, vol. 29, no. 8, pp. 2349–2362, 2019.

[6] K. He, J. Sun, and X. Tang, "Single image haze removal using dark channel prior," *IEEE Transactions on Pattern Analysis and Machine Intelligence*, vol. 33, no. 12, pp. 2341–2353, 2011.

[7] Y. Zhang, P. Wang, Q. Fan, F. Bao, X. Yao, and C. Zhang, "Single image numerical iterative dehazing method based on local physical features," *IEEE Transactions on Circuits and Systems for Video Technology*, vol. 30, no. 10, pp. 3544–3557, 2020.

[8] D. Berman, T. Treibitz, and S. Avidan, "Single image dehazing using haze-lines," *IEEE Transactions on Pattern Analysis and Machine Intelligence*, vol. 42, no. 3, pp. 720–734, 2020.

[9] M. Ju, C. Ding, Y. J. Guo, and D. Zhang, "Idgcp: Image dehazing based on gamma correction prior," *IEEE Transactions on Image Processing*, vol. 29, pp. 3104–3118, 2020.

[10] W. Ren, S. Liu, H. Zhang, J. Pan, X. Cao, and M.-H. Yang, "Single image dehazing via multi-scale convolutional neural networks," in *European conference on computer vision*. Springer, 2016, pp. 154–169.

[11] X. Liu, Y. Ma, Z. Shi, and J. Chen, "Griddehazenet: Attention-based multi-scale network for image dehazing," in *2019 IEEE/CVF International Conference on Computer Vision (ICCV)*, 2019, pp. 7313–7322.

[12] J.-L. Yin, Y.-C. Huang, B.-H. Chen, and S.-Z. Ye, "Color transferred convolutional neural networks for image dehazing," *IEEE Transactions on Circuits and Systems for Video Technology*, vol. 30, no. 11, pp. 3957–3967, 2020.

[13] X. Zhang, T. Wang, W. Luo, and P. Huang, "Multi-level fusion and attention-guided cnn for image dehazing," *IEEE Transactions on Circuits and Systems for Video Technology*, 2020.

[14] Y. Liu, J. Pan, J. Ren, and Z. Su, "Learning deep priors for image dehazing," in *2019 IEEE/CVF International Conference on Computer Vision (ICCV)*, 2019, pp. 2492–2500.

[15] B. Li, Y. Gou, J. Z. Liu, H. Zhu, J. T. Zhou, and X. Peng, "Zero-shot image dehazing," *IEEE Transactions on Image Processing*, vol. 29, pp. 8457–8466, 2020.

[16] Y. Qu, Y. Chen, J. Huang, and Y. Xie, "Enhanced pix2pix dehazing network," in *2019 IEEE/CVF Conference on Computer Vision and Pattern Recognition (CVPR)*, 2019, pp. 8152–8160.

[17] J. Park, D. K. Han, and H. Ko, "Fusion of heterogeneous adversarial networks for single image dehazing," *IEEE Transactions on Image Processing*, vol. 29, pp. 4721–4732, 2020.

[18] J. Pan, J. Dong, Y. Liu, J. Zhang, J. Ren, J. Tang, Y. W. Tai, and M.-H. Yang, "Physics-based generative adversarial models for image restoration and beyond," *IEEE Transactions on Pattern Analysis and Machine Intelligence*, 2020.

[19] S. Kanti Dhara, M. Roy, D. Sen, and P. Kumar Biswas, "Color cast dependent image dehazing via adaptive airlight refinement and non-linear color balancing," *IEEE Transactions on Circuits and Systems for Video Technology*, vol. 31, no. 5, pp. 2076–2081, 2021.

[20] W. Wang, X. Yuan, X. Wu, and Y. Liu, "Fast image dehazing method based on linear transformation," *IEEE Transactions on Multimedia*, vol. 19, no. 6, pp. 1142–1155, 2017.

[21] Y. Bahat and M. Irani, "Blind dehazing using internal patch recurrence," in *2016 IEEE International Conference on Computational Photography (ICCP)*, 2016, pp. 1–9.

[22] T. Cormen, C. Leiserson, R. Rivest, and C. Stein, *Introduction to Algorithms*, ser. Computer science. McGraw-Hill, 2009.

[23] K. He, J. Sun, and X. Tang, "Guided image filtering," *IEEE Transactions on Pattern Analysis and Machine Intelligence*, vol. 35, no. 6, pp. 1397–1409, 2013.

[24] H. Dong, J. Pan, L. Xiang, Z. Hu, X. Zhang, F. Wang, and M.-H. Yang, "Multi-scale boosted dehazing network with dense feature fusion," in *2020 IEEE/CVF Conference on Computer Vision and Pattern Recognition (CVPR)*, 2020, pp. 2154–2164.

[25] M. Sulami, I. Glatzer, R. Fattal, and M. Werman, "Automatic recovery of the atmospheric light in hazy images," in *2014 IEEE International Conference on Computational Photography (ICCP)*. IEEE, 2014, pp. 1–11.

[26] B. Li, W. Ren, D. Fu, D. Tao, D. Feng, W. Zeng, and Z. Wang, "Benchmarking single-image dehazing and beyond," *IEEE Transactions on Image Processing*, vol. 28, no. 1, pp. 492–505, 2019.

[27] C. O. Ancuti, C. Ancuti, R. Timofte, and C. De Vleeschouwer, "O-haze: a dehazing benchmark with real hazy and haze-free outdoor images," in *Proceedings of the IEEE conference on computer vision and pattern recognition workshops*, 2018, pp. 754–762.

[28] C. Ancuti, C. O. Ancuti, R. Timofte, and C. De Vleeschouwer, "I-haze: a dehazing benchmark with real hazy and haze-free indoor images," in *International Conference on Advanced Concepts for Intelligent Vision Systems*. Springer, 2018, pp. 620–631.

[29] A. Mittal, R. Soundararajan, and A. C. Bovik, "Making a completely blind image quality analyzer," *IEEE Signal Processing Letters*, vol. 20, no. 3, pp. 209–212, 2013.

[30] Z. Wang, A. Bovik, H. Sheikh, and E. Simoncelli, "Image quality assessment: from error visibility to structural similarity," *IEEE Transactions on Image Processing*, vol. 13, no. 4, pp. 600–612, 2004.